

to Gallart et al. (1999b). The completeness and error simulation has been performed using a preliminary crowding test table obtained from the deep VLT imaging for Fornax presented in Gallart et al. (2002).

The resulting synthetic CMD is displayed in Figure 6, to the right of the observed CMD. The synthetic CMD successfully reproduces the major morphological features of the observed CMD, namely the RGB, the horizontal branch, the red-clump and the main-sequence. Particularly important is the agreement between locations of the young main-sequence stars (a set of lines have been drawn in both the observed and model CMDs to guide the eye). Its position is very sensitive to metallicity of the stars younger than about 2 Gyr. If their metallicity were lower than that given by the $Z(t)$ relation, for example, lower than $[Fe/H] \leq -0.7$, as one could deduce from the color of the RGB without correction for the young ages of the stars, then the position of this part of the main sequence would be substantially too blue. There is also striking agreement between the model and observed CMDs for the *plume* of stars above the red-clump, which is composed of metal rich young stars (younger than 1 Gyr and with $Z \approx 0.006-0.008$) undergoing their He-burning loop phase of stellar evolution. The most obvious disagreement between the model and the observed CMDs is in the color of the RGB. To illustrate this we have plotted in both diagrams the fiducial RGBs of the globular clusters M15, M2, NGC 1851 and 47

Tuc, from Da Costa & Armandroff (1990). Notice that the model RGB is somewhat redder than the observed one. This disagreement, which is larger for the fainter RGB stars, is known to exist from other comparisons between observations and the Padova stellar evolutionary models. It has no effect on our major conclusion that the $Z(t)$ shown in Figure 5 is compatible with the morphology of the Fornax CMD. A quantitative derivation of the star formation history from a thorough fit of the CMD will add further confidence in the reconstruction of the history of Fornax. It will be presented in Gallart et al. (2002).

Acknowledgements. This research is part of a Joint Project between Universidad de Chile and Yale University, funded partially by the Fundación Andes. C.G. acknowledges partial support from Chilean CONICYT through FONDECYT grant number 1990638. R.Z. was supported by NSF grant AST-9803071 and F.P. by the Swiss National Science Fund and FONDECYT grant number 3000056.

References

- Aaronson, M., Olszewski, E.W. & Hodge, P.W. 1983, *ApJ*, **267**, 271
 Aaronson, M. & Mould, J. 1980, *ApJ*, **240**, 804
 Aparicio, A., Carrera, R. & Martínez-Delgado, D. 2001, *AJ*, **122**, 2524
 Bertelli, G., Bressan, A., Chiosi, C., Fagotto, F. & Nasi, E. 1994, *A&AS*, **106**, 275
 Bertelli, G. et al. 2002, in preparation
 Bonifacio, P., Hill, V., Molaro, P., Pasquini, L., Di Marcantonio, P., & Santin, P. 2000, *A&A*, **359**, 663

- Buonanno, R., Corsi, C.E., Castellani, M., Marconi, G., Fusi Pecci, F. & Zinn, R. 1999, *AJ*, **118**, 1671
 Cannon, R.D., Niss, B. & Norgaard-Nielsen, H.U. 1981, *MNRAS*, **196**, 1
 Caputo, F., Cassisi, S., Castellani, M., Marconi, G., Santolamazza, P. 1999, *AJ*, **117**, 2199
 Carrera, R., Aparicio, A., Martínez-Delgado, D., & Alonso, J. 2002, *AJ*, in press
 Castellani, M., Pulone, L., Ripepi, V., Dal'Orta, M., Bono, G., Brocato, E., Caputo, F., Castellani, V., Corsi, C. 2001, in "Dwarf Galaxies and their environment", eds. K.S. de Boer, R.-J. Dettmar & U. Klein, Shaker Verlag.
 Cole, A., Smecker-Hane, T.A., Gallagher, J.S. 2000, *AJ*, **120**, 1808
 Da Costa, G. S. & Armandroff, T. E. 1990, *AJ*, **100**, 162
 Demers, S. & Kunkel, W.E. 1979, *PASP*, **91**, 761
 Gallart, C., Aparicio, A., Bertelli, G. 2002, in "Observed HR diagrams and stellar evolution...", eds. T. Lejeune & J. Fernandes, ASP Conference Series.
 Gallart, C. et al. 1999a, *ApJ*, **514**, 665
 Gallart, C., Freedman, W.L., Aparicio, A., Bertelli, G. & Chiosi, C. 1999b, *AJ*, **118**, 2245
 Gallart, C., Zinn, R., Marconi, G., Hardy, E. & Buonanno, R. 2002, in prep.
 Hurley-Keller, D., Mateo, M. & Nemeč, J. 1998, *AJ*, **115**, 1840
 Kroupa, P., Tout, C.A. & Gilmore, G. 1993, *MNRAS*, **262**, 545
 Norris, J. & Zinn, R. 1975, *ApJ*, **202**, 335
 Pont, F., Zinn, R., Gallart, C., Winnick, R., Hardy, E. 2002, in preparation
 Shetrone, M.D., Côté, P. & Sargent, W.L.W. 2001, *ApJ*, **548**, 592
 Smecker-Hane, T. A., Stetson, P. B., Hesser, J. E. & van den Bergh, D. A. 1996 in *From stars to galaxies...*, eds.
 C. Leitherer, U. Fritze-van Alvensleben & J. Huchra. ASP Conf Ser, **98**, 328
 Stetson, P. B., Hesser, J. E. & Smecker-Hane, T. A. 1998, *PASP*, **110**, 533

The ups and downs of a stellar surface: Nonradial pulsation modelling of rapid rotators

THOMAS RIVINIUS, DIETRICH BAADE, ESO, Garching b. München, Germany

STANISLAV ŠTEFL, Astronomical Institute, Academy of Sciences Ondřejov, Czech Republic,

MONIKA MAINTZ, Landessternwarte Heidelberg, Germany

RICHARD TOWNSEND, University College London, United Kingdom

1. Introduction

Usually one thinks of stars as stable objects, taking at least millions of years to evolve significantly. While it is true that stars take such timescales to age, they need not be "stable" in a static sense over all that time. Many stars in fact undergo pulsations on timescales between minutes and years, as for instance the Be stars Baade, Rivinius and Štefl reported about in a recent *Messenger* issue (No. 107, p. 24). The most obvious pulsation mode is the radial one, where the star becomes bigger and smaller periodically, and like

any expanding/compressing gas also cooler and hotter again. We see these stars varying in brightness and colour, and their spectra cyclically approaching and receding. The well known Mira in the constellation Cetus ($P = 330$ day), or the Cepheids ($P = 1...50$ day), which help in measuring extragalactic distances, are such objects. Stars may not only pulsate radially, however. Imagine a free-floating blob of water in a Space Shuttle, or a big soap bubble. Before reaching a stable spherical shape (or popping) they undergo damped wobbles. This, in a sense, is externally excited non-

radial pulsation (*nrp*) in a multitude of modes.

Nonradially pulsating stars behave similarly. But since these pulsations are excited from inside the star and are going on for millions of cycles, they appear more ordered as most modes are damped, and typically only one or few high-amplitude modes are excited in an *nrp* star. The excitation process resembles a Carnot process (as in an ideal steam engine) where the role of the valve is played by a layer inside the star that turns opaque with increasing temperature due to ionization processes and becomes transparent again during

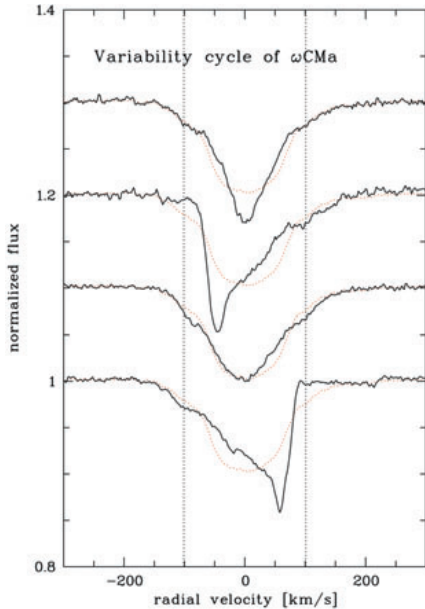


Figure 1: The pulsational variability of ω CMA in the MgII 4481 line. The phase (i.e. time) increases from bottom to top. The mean profile, which is averaged over all pulsation phases, is shown in red, the projected rotation velocity of the star is plotted as dotted lines, shifted to the stellar systemic velocity. The range of variability exceeds the rotational range by about 40 km s^{-1} with a ramp-like form. The line profile variability, well seen also in the asymmetric “spikes” at the most extreme blue and red phases, is among the strongest ever observed.

the following expansion phase. When such a layer is close to the stellar surface, stellar pulsation may be excited. On the stellar surface *nrp* manifests itself as a global wave pattern, which travels along the stellar surface parallel to the equator and causes the periodic behaviour. This global wave pattern can be described by means of quantum numbers ℓ and m , characterizing the number of oscillation nodes along the equator and across it, similar to the two-dimensional oscillations of a drumskin (or of the VLT primary mirror, being exploited for the active optics).

Such *nrp* might be very subtle, as in our Sun, which pulsates in numerous low-amplitude modes with $P = 5 \text{ min}$. In other stars, like the Be stars, however, the induced variability may look so violent, that it was first claimed that, if this were pulsation, the star would be disrupted. In fact, browsing the spectra of the early type Be star ω CMA after the observations taken during the HEROS project (Fig. 1, see also Baade et al., op. cit.), we were convinced that the periodic variability could not be modelled without taking into account also shocks and other non-linear effects. Most notably, the variability can be observed out to higher velocities than the projected stellar rotational velocity, which would normally suggest a

circumstellar origin, and the strong, narrow absorption “spikes” seemed to require severe distortions of the stellar surface (see Fig. 1 for an example). However, as will be shown, these features could be modelled without any additional assumptions with a general-purpose non-radial pulsation modelling code.

Other hypotheses proposed to explain the line profile variability (*lpv*) of Be stars, and especially of ω CMA, include starspots and co-rotating clouds. However, for none of them was a satisfying model able to reproduce the observed variations of more than a single spectral line.

Ever since the discovery of periodic *lpv* in Be stars one has wondered whether it could be the same process that is responsible for building up the circumstellar disk. Since the mass loss modulations of early type stars are not very well understood in general, the identification of the cause of the *lpv* in Be stars also would be a step forward in hot star physics in general.

2. A new model-code

When the HEROS project started, none of the hypotheses introduced above was clearly favoured. At this point, however, a new *nrp* modelling code, the BRUCE/KYLIE-package, was published by Rich Townsend. Several advantages made it the first choice to attempt modelling the *lpv* of ω CMA (and other pulsating Be stars).

For instance, the pulsational surface wave pattern depends not only on ℓ and m , but also on stellar rotational velocity. With increasing rotation, the wave pattern becomes more and more concen-

trated towards the equator. BRUCE, other than most codes before, can compute the surface wave pattern up to the critical rotation limit. It is therefore ideally suited to Be stars, that typically rotate at about 70 to 80% of their critical speed.

Also, BRUCE is one of the few codes optimized for relatively long oscillation periods (i.e. longer than the fundamental radial oscillation mode), for which horizontal motions are the most important. These are called *g*-modes (since gravity is the most important restoring force) and are comparable to water waves in an ocean. Most other codes specialize in short period pulsation modes, where radial motions dominate, called *p*-modes (from pressure) and rather resembling sound waves.

The input parameters required by BRUCE are stellar quantities (mass, temperature, radius, rotation, and inclination), and the pulsational parameters. At first look, this seems to be a disadvantage of the code, because other codes require only the pulsational parameters, but also only compute the variability of the *residuals* from the mean, not the line profiles themselves. However, this is in fact a major advantage, since the variability depends strongly on properties of the spectral line modelled, which in turn are determined by the stellar parameters. The extended wavelength range of echelle data allows one to make use of the differences of individual spectral lines formed at different stellar latitudes to further constrain the model parameters. Therefore, the reproduction of the variability and the mean profile, for as many different lines as possible, not only gives the pulsational parameters, but also the stellar ones.

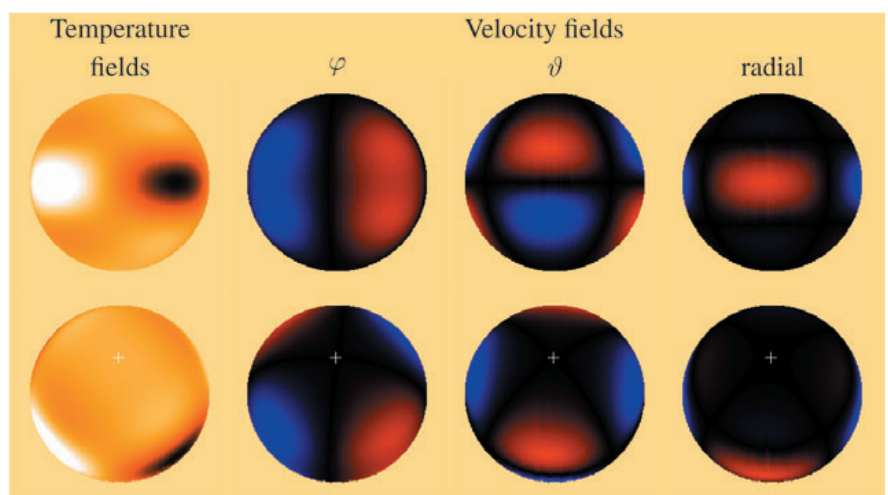


Figure 2: The pulsational variations of the stellar surface as computed by BRUCE for an $\ell = 2$, $m = 2$ mode. This sectorial mode has two node-lines in longitude ($\ell = 2$), thus the *nrp*-pattern repeats twice along the equator. The same model is shown for equator-on (upper row) and almost pole-on orientation, like ω CMA is seen from Earth (lower row, the “+” marks the rotational pole). The radial motions are a factor of almost 10 slower than the horizontal ones, while the ϕ - and θ -amplitudes are about equal. These three velocity fields are co-added and projected onto the line of sight, before KYLIE computes the observed spectrum (see also Fig. 3). The temperature changes are caused by the varying pressure.

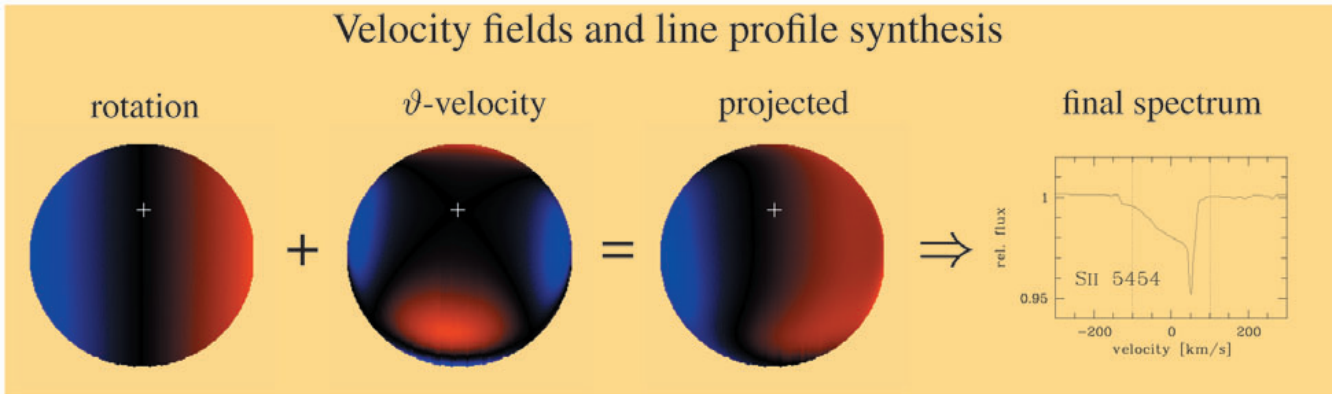


Figure 3: The projected velocity field, as seen from Earth, is dominated by the rotation and the pulsational θ -velocity for a pole-on star. At the approaching limb of the star (blue), the co-added θ -amplitude increases the total approaching velocity, causing the extended ramp on the blue wing of the final spectrum (see also Fig. 1). At the receding limb, rotation and θ -velocity have different signs, thereby reducing the maximal projected velocity. A large part of the receding hemisphere is, therefore, projected into a narrow velocity range, causing the spike. The modelled SiII 5454 line is shown for illustration.

BRUCE computes the surface parameters (such as temperature, gravity, and projected velocity) of the pulsating star for a mesh of about 25,000 points on the visible surface (Fig. 2 has been constructed from the BRUCE output). For each surface point the local spectrum is taken from an input grid of pre-computed data and shifted by the projected velocity. The KYLIE program then co-adds these local spectra to the one that would be observed from Earth.

3. Reproducing spectra

How could this new code help in resolving the seemingly contradictory behaviour of ω CMa? The key is the almost polar inclination of the star. Figure 2 shows the three constituents of the pulsational velocity before projection

onto the line of sight. In the equatorial view, the ϕ -velocity would dominate the visible variability at the stellar limbs. The θ -component is almost perpendicular to the line of sight, and thus suppressed by projection effects in the equatorial view. For a polar orientation of the star, the situation is reversed, however. The θ -velocity is now dominant, while the visibility of the ϕ -component is suppressed. Since the rotational velocity is also in ϕ -direction, it underlies the same projection.

The excess of 40 km s^{-1} , by which the variability is seen beyond the rotational range (such features are also called ramps), is therefore the true maximal velocity of the θ -field. Since this is 40% of the *projected* rotational velocity at the small inclination of ω CMa, it alters the visible line profile sig-

nificantly (see Fig. 3). But it is only about 15% of the *true* rotational velocity, so the physical effects on the stellar surface are much less severe. This way the polar inclination amplifies the contrast of the observed variability for g -mode pulsation.

Figure 3 demonstrates how under these conditions ramps and spikes result from the generic properties of a nonradially oscillating, rotating sphere, without the necessity to customize the model code for the specific case of ω CMa.

The final parameter set to reproduce the spectral variability of ω CMa was searched by computing and testing tens of thousands of models against the observations. The recent Messenger article by Baade et al. (*op. cit.*) has already presented an example of

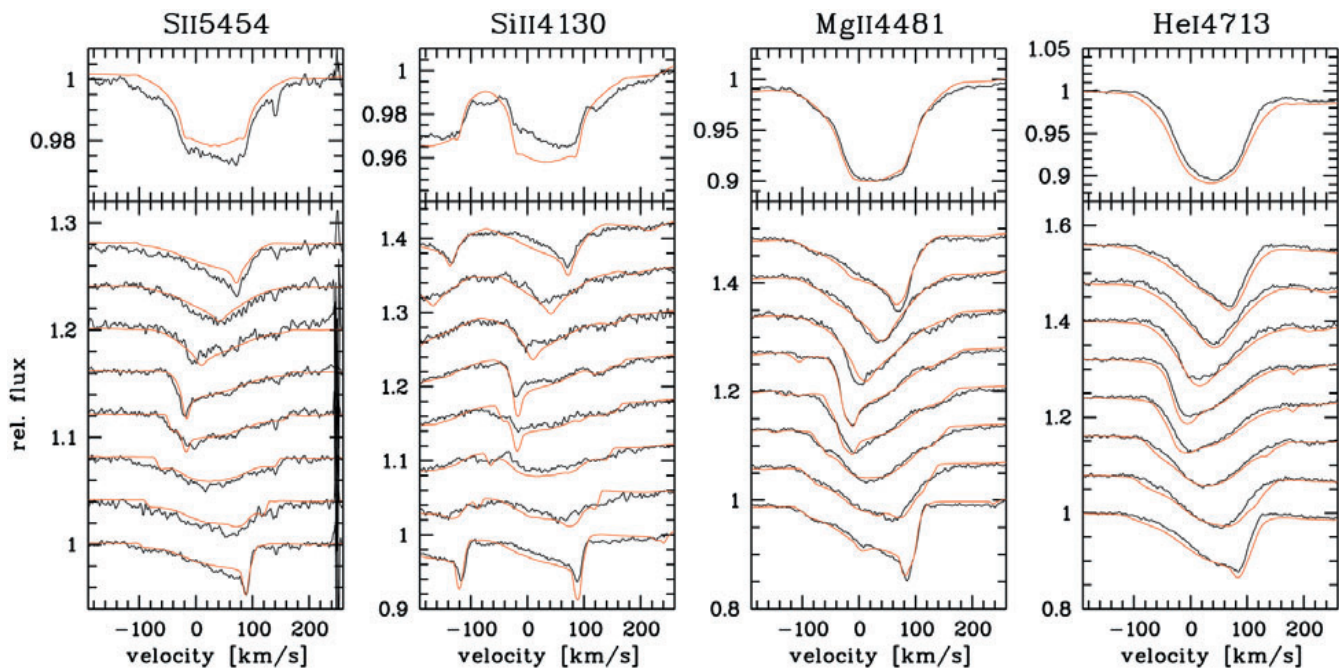


Figure 4: Comparison of observed phase-variations (black) with the modelled ones (red), including line blends. The phase averaged mean spectra are plotted above. The good reproduction, also of the absolute mean line profiles (and their anomalies, like the flat bottoms), demonstrates that the stellar parameters derived by modelling the variability provide a good estimate of the true quantities.

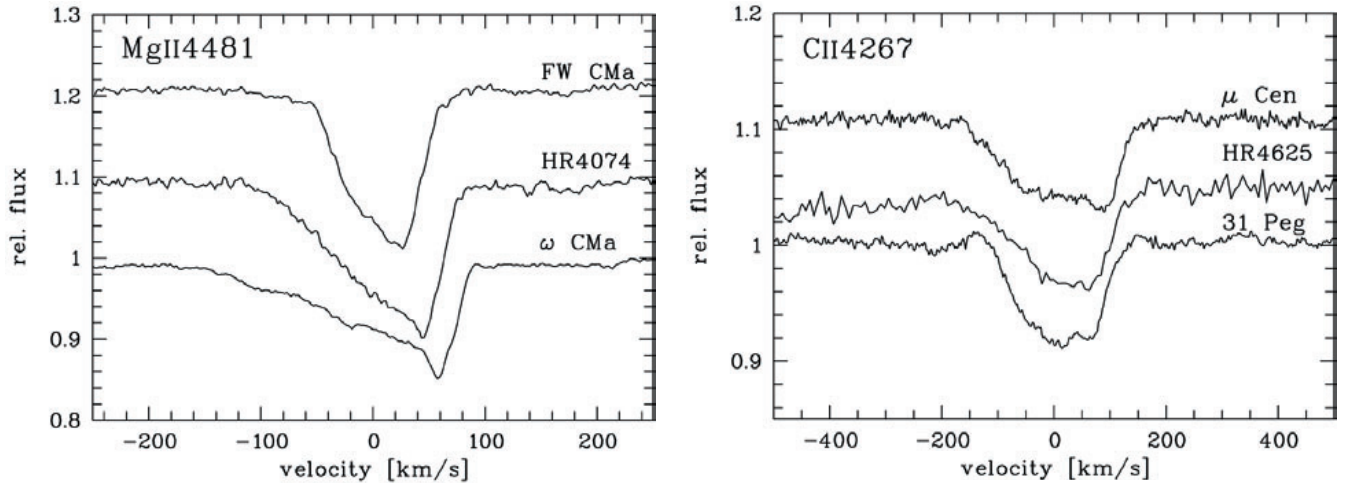


Figure 5: Periodic line profile variability (lpv) of low $v \sin i$ Be stars shown in the extreme asymmetry phase. The lpv of ω CMa is the strongest, but not in principle different from other low $v \sin i$ Be stars. See also Figure 6 for a dynamical view of the lpv of FW CMa, ω CMa, and HR 4625.

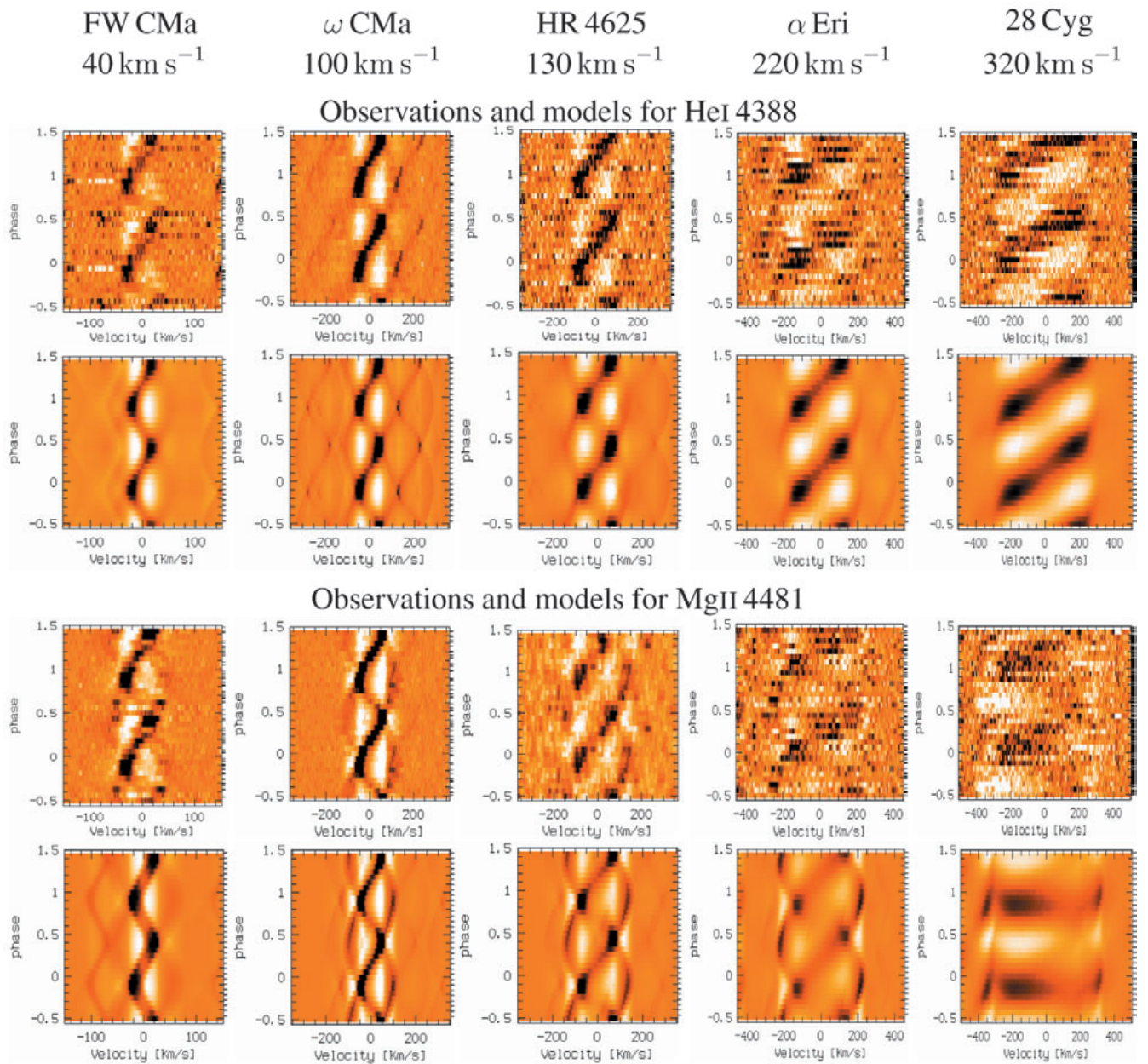


Figure 6: Observed lpv of stars with different $v \sin i$, shown as residuals from the mean line profile for two different lines. It is compared to the ω CMa model being 'viewed' at inclinations between 6° and 70° to match the indicated $v \sin i$ of the observed stars. The apparently asymmetric lpv of Mg II 4481 in 28 Cyg is caused by rotational blending with HeI 4471, visible in both observations and model data.

the resulting reproduction of the l_{pv} of HeI 4471 and MgII 4481. In Fig. 4, results for additional lines of helium and other ions are shown, all computed with the same set of stellar and pulsational parameters.

4. Do all Be stars pulsate?

Since the periodic l_{pv} of ω CMa is among the strongest known, the question needs to be addressed whether it is a typical Be star.

ω CMa is a B2 IV star. Since it is known that Be stars rotate almost critically, its low projected rotational velocity $v \sin i$ points to a pole-on orientation, which is also supported by the derived model parameters. If all (or most) other such Be stars would show this kind of periodic variability (possibly weaker, but in principle the same), the l_{pv} could be explained by nrp in general.

Although most Be stars are of early B spectral type, there are not too many bright ones in the same range of $v \sin i$ as ω CMa. Searching archival data and securing additional observations with FEROS, we found most of them to show spikes like ω CMa, or a similar variability with lower amplitudes, i.e. no fully developed spikes, but global asymmetry variations, as is shown in Figure 5.

A complementary approach focuses on the observed l_{pv} of equator-on (high $v \sin i$) stars. The l_{pv} of these stars looks different from the pole-on ω CMa. But if ω CMa is proto-typical, the differences should be just inclination effects. To address this expectation the model of ω CMa was computed for a set of inclinations, so that the resulting $v \sin i$ would be the same as for some typical Be stars. Then, the modelled variations were compared to the observed ones (Fig. 6). The similarity of model and observations shows that the model of ω CMa represents a typical early-type Be star.

5. Consequences and outlook

The main result of the modelling project is the confirmation that early-type Be stars pulsate nonradially in g -modes. Based on the detailed modelling of ω CMa, it could be shown that this star is proto-typical, and that the periodic l_{pv} of early type Be stars in general is due to nonradial pulsation.

Several stars in the database, including ω CMa, were observed to replenish their disks via outburst events during our campaigns. Although plain nrp cannot account for mass and angular momentum transfer into the disk, there is

observational evidence for a connection between nrp and the disk formation. Among other effects, the l_{pv} pattern of ω CMa changes in several spectral lines during an outburst, which might provide the key to understand the mass transfer mechanism between Be stars and their disks.

Just as the pulsational parameters are determined by the best fit of the variability, the stellar parameters can be determined by the best fit of the mean absolute line profile. The modelling method described above offers the potential to combine these two steps in a single analysis, due to the good reproduction of both residual variability and absolute line profile (see Fig. 6). Since nonradial pulsation breaks the symmetry of the stellar surface w.r.t. rotation, one can even derive the stellar inclination angle from the modelling, while otherwise it is inseparably factored into the projected rotational velocity $v \sin i$. Rotation is becoming increasingly important for understanding stellar structure and evolution. A method to derive v and i separately, utilizing the nrp pattern on the stellar surface, bears great potential not only for Be stars, but for a much wider range of objects, since nonradial pulsation is widespread in the Hertzsprung-Russell-Diagram.

The VLT and the most distant quasars

L. PENTERICCI and H.W. RIX (MPIA, Heidelberg), X. FAN (IAS Princeton), M. STRAUSS (Princeton University)

1. Introduction: optical surveys for high-redshift quasars

Quasars are amongst the most luminous objects in the Universe, allowing us to study them and any intervening material out to very large distances, corresponding to look-back times when the Universe was very young. Finding and studying quasars at high redshifts is one of the best ways to constrain the physical conditions in the early Universe. The mere existence of luminous quasars at such early times, and the implied presence of black holes with $M \geq 10^9 M_{\odot}$ place stringent limits on the epoch at which massive condensed structures formed, thereby constraining structure formation models (e.g. Efsthathiou and Rees 1988).

Most known high redshift quasars have been found as outliers in color space from the stellar locus in multicolor or optical surveys (e.g. Warren et al. 1994, Kennefick et al. 1995). One prominent survey is the Sloan Digital Sky Survey (SDSS, York et al. 2000) which is systematically mapping one-

quarter of the entire sky, producing a detailed multi-color image of it and determining the positions and absolute brightnesses of more than 100 million celestial objects. The SDSS will also measure the distance to a million of the nearest galaxies, producing a three-dimensional picture of the Universe through a volume one hundred times larger than that explored to date.

One of the principal aims of the SDSS is the construction of the largest sample of quasars ever, with more than 100,000 objects spanning a large range of redshift and luminosities, giving us an unprecedented hint at the distribution of matter to the edge of the visible Universe.

Thanks to the accurate 5 band photometry of SDSS, high redshift quasars can be efficiently selected by their distinctive position in color-color diagrams, with characteristic colors due to the main feature of the quasar spectra, viz., the strong Ly α emission line, the Ly α forest and the Lyman limit. During its first year of operation, the SDSS has already found a large number of ex-

tremely distant quasars, including more than 200 new quasars at redshift greater than 4 and the most distant quasar known, SDSS J1030 + 0524 at $z = 6.28$ (Fan et al. 2001). Until a few months ago this was also the most distant object known but it has been surpassed by a galaxy at $z = 6.56$ recently discovered by Hu et al. (2002).

2. VLT observations of the most distant quasars: revealing the conditions of the early Universe

The spectra of very high redshift quasars can tell us a great deal about the conditions in the early Universe. In particular, we can use them as probes of the intergalactic medium (IGM) to determine the state of any intervening material along the line of sight.

One of the fundamental questions of modern cosmology is how and when the Universe became ionized (for a complete review see Loeb & Barkana 2001). When the Universe was very